High precision measurement of the ^{87}Rb D-line tune-out wavelength

R. H. Leonard,[1] A. J. Fallon,[1] C. A. Sackett,[1] and M. S. Safronova[2, 3]

[1] *Physics Department, University of Virginia, Charlottesville, Virginia 22904, USA*
[2] *Department of Physics and Astronomy, University of Delaware, Newark, Delaware 19716, USA*
[3] *Joint Quantum Institute, National Institute of Standards and Technology and the University of Maryland, College Park, Maryland, 19716 USA*

(Dated: July 30, 2015)

We report an experimental measurement of a light wavelength at which the ac electric polarizability equals zero for ^{87}Rb atoms in the $F = 2$ ground hyperfine state. The experiment uses a condensate interferometer both to find this 'tune-out' wavelength and to accurately determine the light polarization for it. The wavelength lies between the D1 and D2 spectral lines at 790.03235(3) nm. The measurement is sensitive to the tensor contribution to the polarizability, which has been removed so that the reported value is the zero of the scalar polarizability. The precision is fifty times better than previous tune-out wavelength measurements. Our result can be used to determine the ratio of matrix elements $\left|\langle 5P_{3/2}||d||5S_{1/2}\rangle/\langle 5P_{1/2}||d||5S_{1/2}\rangle\right|^2 = 1.99219(3)$, a 100-fold improvement over previous experimental values. Both the tune-out wavelength and matrix element ratio are consistent with theoretical calculations, with uncertainty estimates for the theory about an order of magnitude larger than the experimental precision.

PACS numbers: 03.75.Dg,37.25.+k,42.50.Wk

The energy shift experienced by an atom in an off-resonant optical field has found numerous applications in atom trapping, manipulation, and measurement. The light shift can be characterized by a frequency-dependent polarizability, which itself depends in detail on the wave function of the electrons in the atom. Accurate measurements of the polarizability can therefore be used to test atomic theory calculations, or as phenomenological inputs to improve those calculations. Polarizability measurements have a long history of improving our knowledge of atoms in this way [1, 2].

Precise measurements of the polarizability at optical frequencies are technically difficult, because the light shift depends also on the optical intensity and it is hard to accurately determine the intensity *in situ*. However, it is possible to instead measure a light wavelength at which the polarizability equals zero [3–5]. Since these tune-out wavelengths are independent of the intensity, they can be accurately measured by various methods [5–9].

Tune-out wavelengths can be useful for applications involving species-specific optical manipulation [3, 4, 6, 10] and optical Feshbach resonances [9]. In addition, it was recently shown that tune-out wavelengths can be used with an atom interferometer for sensitive detection of rotations and accelerations [11]. Improved knowledge of tune-out wavelengths can lead to better performance in all these applications.

In this Letter we report measurement of the tune-out wavelength for ^{87}Rb near 790 nm, with an accuracy of about 30 fm. This can be compared to the 1.5 to 2 pm precision of previously reported values for this [6] or other tune-out wavelengths [5, 7, 8]. Our result determines the ratio of the D-line dipole matrix elements to an accuracy of 15 ppm, about a factor of 100 better than previously known [27]. At our precision the measurement is sensitive to many new effects including hyperfine interactions [13], QED effects [14], the Breit interaction [15], and the details of the atomic core and core-valence interactions [4]. The theoretical tools required to handle these challenges are similar to those needed to interpret results such as atomic parity violation and electric dipole measurements in terms of fundamental particle properties [16]. Similar calculations are also useful for constraining black-body radiation shifts in atomic clocks [17]. Our measurement can thus serve as a useful test for theories, or could be taken as a phenomenological input value for improved results.

For an alkali atom in state i, the polarizability can be expressed (in atomic units) as

$$\alpha_i(\omega) = \sum_f \frac{2\omega_{if}}{\omega_{if}^2 - \omega^2} |d_{if}|^2 + \alpha_{\rm core} \qquad (1)$$

where the sum is over all excited states f of the valence electron, ω_{if} is the transition frequency between i and f, and $d_{if} = \langle f|\mathbf{d}\cdot\hat{\epsilon}|i\rangle$ is the dipole matrix element between i and f for light with polarization vector $\hat{\epsilon}$. The remaining term $\alpha_{\rm core}$ incorporates the polarizability contributions from the core electrons as well as core-valence interactions [4]. At most frequencies, it is small compared to the valence contribution. However, tune-out wavelengths occur between pairs of states where the valence contributions largely cancel. Figure 1(a) shows the tune-out wavelength between the D1 and D2 lines of Rb.

Our measurement uses a Bose condensate atom interferometer, similar to that previously described in [18]. A condensate of about 10^4 ^{87}Rb atoms is produced and loaded into a weak magnetic trap with harmonic oscillation frequencies of 5.1, 1.1, and 3.2 Hz along the x, y, and z directions, respectively. The trap uses a time-orbiting potential, with a bias field of about 20 G rotating in the xz plane at 12 kHz frequency. Oscillating magnetic

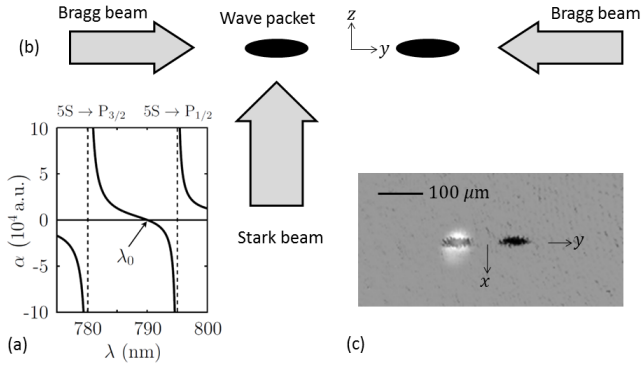

FIG. 1: Schematic of measurement. (a) Theoretical plot of the polarizability α for ^{87}Rb near the D1 and D2 transitions. The polarizability crosses zero at the tune-out wavelength λ_0. (b) Optical schematic for the experiment. The two Bragg laser beams form a standing wave that is used to split and recombine a Bose condensate to form an atom interferometer. The Stark laser beam illuminates one of the wave packets in the interferometer to produce a phase shift. (c) Composite image of the atomic wave packets (dark) and the Stark beam (white). Here the wave packet centers are 130 μm apart after 5 ms of propagation. In (b) and (c), the coordinate axes x, y and z are illustrated.

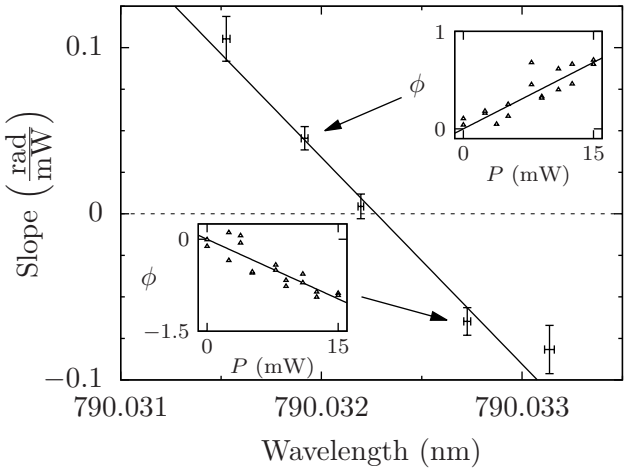

FIG. 2: Sample data. The two inset graphs show interferometric measurements of the phase shift ϕ induced by the Stark beam with power P. The triangles show individual measurements, which are fit to a line to determine the slope. The large graph shows how the slope varies as a function of the Stark laser wavelength, with the inset graphs corresponding to the indicated points. The vertical error bars are the linear regression errors from the slope fits. The horizontal error bars are the standard deviation of several wavelength readings made over the course of the measurement. The line in the large graph is another linear fit, and the intercept is taken as our measurement result for the tune-out wavelength λ_0. Here $\lambda_0 = 790.03228$ nm, with a regression error of 50 fm.

gradients provide support against gravity as well as trap confinement.

The atom interferometer is implemented using an off-resonant standing-wave laser propagating along the y axis, having wave number k. Via Bragg scattering, a short pulse from this beam can split the atoms into two wave packets traveling with momentum $\pm 2\hbar k$ [19]. After 10 ms, the wave packets are reflected using another pulse of the Bragg laser, now adjusted to drive the $|+2\hbar k\rangle \leftrightarrow |-2\hbar k\rangle$ transition. After 20 ms a second reflection pulse is applied, and after another 10 ms, a recombination pulse is applied. By using this symmetric trajectory, both packets traverse identical paths in the trap, which reduces phases shifts and fidelity loss from the trapping potential [18].

The recombination pulse brings a fraction N_0/N of the atoms back to rest in the center of the trap. We obtain $N_0/N = [1 + V\cos(\phi + \phi_r)]/2$, where ϕ is the phase difference developed by the atoms during their separation, ϕ_r is the phase shift of the recombination pulse relative to the initial splitting pulse, and $V \approx 0.7$ is the visibility. We here set $\phi_r = \pi/2$ to maximize the sensitivity to ϕ. We measure N_0/N by allowing the three output wave packets to separate for 40 ms and then observing them via absorption imaging.

To obtain the polarizability α, we focus another laser beam, traveling along z, onto one arm of the interferometer. This Stark beam is applied for 20 ms at the start of the interferometer, so that one packet passes through it twice. Figure 1(b) shows the orientation of the beams involved, and Fig. 1(c) is a composite image of the atoms and Stark beam together.

The energy shift U due to the Stark beam is

$$U = -\frac{1}{2}\alpha\left\langle E^2\right\rangle = -\frac{2\pi}{c}\alpha I \qquad (2)$$

where E is the electric field of the beam, I is the intensity, and c is the speed of light. The brackets denote time averaging of the optical field. The light shift induces a phase $\phi = -\int U dt$ proportional to the integrated intensity experienced by the atoms. We use an approximately Gaussian beam with waist $w \approx 30$ μm. For a Stark beam power of P, this yields $\phi/(\alpha P) \approx 66$ rad/W for α in atomic units.

The Stark power can be varied from zero to 15 mW using an acousto-optic modulator. The basic experimental procedure is to set the Stark laser to a given wavelength λ and run the interferometer for different beam powers. The resulting phase is fit to a line to determine the slope, as shown in the Fig. 2 insets. By performing the experiment at different wavelengths, we plot the slope as a function of λ. A second linear fit yields the wavelength λ_0 at which the slope and thus α equals zero.

A major complication is that α depends strongly on the polarization of the Stark beam and the orientation of the atomic spin. In general the energy shift can be

expressed as [13]

$$U = -\frac{\langle E^2\rangle}{2}\Bigg\{\alpha^{(0)} + \mathcal{V}\cos\chi\frac{m_F}{2F}\alpha^{(1)} + \left[\frac{3\cos^2\xi - 1}{2}\right]\frac{3m_F^2 - F(F+1)}{F(2F-1)}\alpha^{(2)}\Bigg\} \tag{3}$$

where the $\alpha^{(i)}$ are irreducible components of the polarizability, namely the scalar ($i = 0$), vector ($i = 1$) and tensor ($i = 2$) parts. The atom is assumed to be in a particular hyperfine state $|F, m_F\rangle$ relative to the trap magnetic field direction $\hat{b} = \mathbf{B}/B$. Here we have $F = m_F = 2$. The Stark beam propagates at angle χ with respect to the magnetic field, and $\cos\xi$ is the projection of the light polarization vector $\hat{\epsilon}$ onto the magnetic field, $\cos\xi = \hat{\epsilon}\cdot\hat{b}$. Finally $\mathcal{V}$ is the fourth Stokes parameter for the light, characterizing the degree of circular polarization and expressible as $\mathcal{V}\cos\chi = i(\hat{\epsilon}^*\times\hat{\epsilon})\cdot\hat{b}$.

We are primarily interested in the scalar polarizability $\alpha^{(0)}$. The tensor contribution is small but measurable, and will be discussed below. However, the vector contribution can be quite large. For instance, for σ_+ polarized light ($\mathcal{V} = -1$ and $\chi = 0$) the vector term completely eliminates the tune-out wavelength between the D1 and D2 transitions, since the light does not couple our ground state to any states in the D1 manifold. To measure the tune-out wavelength of the scalar term with the desired accuracy, it is necessary to keep $|\mathcal{V}\cos\chi| < 10^{-5}$. This is challenging since it is comparable to the performance of the best linear polarizers, and much below the level of polarization that can typically be maintained when a laser beam passes through a vacuum chamber window.

We use two methods to control the vector shift. First, the rotating bias field of the TOP trap causes $\cos\chi$ in Eq. (3) to alternate sign, with a time average close to zero. We verified that the measurement results did not depend on the phase of the TOP field at the start of the interferometer.

Second, we linearized the light polarization using the interferometer itself. Prior to taking a data set such as in Fig. 2, we ran the experiment with the Stark beam pulsed on and off synchronously with the TOP field. In this way the $\cos\chi$ term could be made close to +1 or -1. We adjusted the light polarization so that the measured phase shifts for those two cases were equal. The polarization was established with a calcite polarizer, a zero-order half wave plate, and a zero-order quarter wave plate. The wave plates could be set to an accuracy of about 0.1°, corresponding to $\mathcal{V} \approx 2\times10^{-3}$.

After taking the data set, the polarization check was repeated and any difference between the $\cos\chi = \pm1$ phases was used to estimate the polarization drift that occurred during the run. This was converted to a wavelength error using an empirical calibration, and the polarization error was added in quadrature to the regression error calculated as in Fig. 2.

The tensor term in (3) gives rise to a dependence on the angle of the linear light polarization with respect to the trap field, which can be seen in Fig. 3. The polarization was adjusted using the half-wave plate in the Stark beam. For our geometry, the polarization angle θ is related to ξ in (3) via $\langle\cos^2\xi\rangle = 0.5\cos^2\theta$, where the brackets denote a time average for the magnetic field.

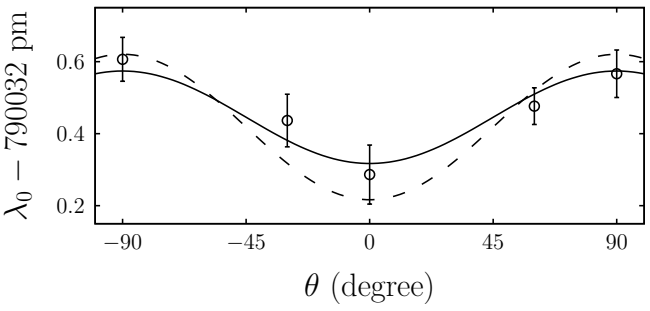

FIG. 3: Effect of tensor polarizability. Data points show tune-out wavelengths λ_0, as a function of the angle θ between the linear polarization of the Stark beam and the x axis of the trap. Each point is an average of several measurements performed as in Fig. 2. For each measurement i the linear fit error is combined with the estimated polarization error described in the text. The error bars shown are then calculated as $\sigma^2 = 1/\sum_i \sigma_i^{-2}$. The solid curve is a sinusoidal fit with a variable offset and amplitude. The dashed curve is a fit with the amplitude constrained to the expected value.

Near the tune-out wavelength, α and $\alpha^{(0)}$ can be approximated as linear functions $(d\alpha/d\lambda)(\lambda - \lambda_0)$ and $(d\alpha^{(0)}/d\lambda)(\lambda - \lambda^{(0)})$ respectively. Here λ_0 is the measured value shown in Fig. 3 and $\lambda^{(0)}$ is the desired zero of the scalar term. The tensor contribution to $d\alpha/d\lambda$ is negligible, so the two derivatives are nearly equal. If we use this and set (3) to zero, we obtain

$$\lambda_0(\theta) = \lambda^{(0)} - \frac{\alpha^{(2)}}{d\alpha^{(0)}/d\lambda}\left(\frac{3}{4}\cos^2\theta - \frac{1}{2}\right) \tag{4}$$

in the case of $\mathcal{V}\langle\cos\chi\rangle = 0$. Fitting to this form, we obtain $\lambda^{(0)} = 790.032403(35)$ nm and $\alpha^{(2)}/(d\alpha^{(0)}/d\lambda) = 390(120)$ fm. This fit is shown as the solid curve in Fig. 3.

Alternatively, $\alpha^{(2)}$ and $d\alpha^{(0)}/d\lambda$ are almost entirely due to contributions from the 5P manifold, and can be calculated relatively precisely. The derivative term can be determined from [13]

$$\alpha^{(0)}_{5P} = \frac{10}{\sqrt{15}}\sum_{J',F'}\frac{|d_{J'}|^2\,\omega'}{\omega'^2 - \omega^2}(-1)^{1+F'}(2F'+1) \times \begin{Bmatrix} 2 & 1 & F' \\ 1 & 2 & 0 \end{Bmatrix}\begin{Bmatrix} F' & 3/2 & J' \\ 1/2 & 1 & 2 \end{Bmatrix}^2 \tag{5}$$

for the $F = 2$ ground state. Here the sum is over the angular momentum quantum numbers of the 5P states, ω' is the transition frequency to the $|J', F'\rangle$ state, and $d_{J'} = \langle 5P_{J'}||d||5S_{1/2}\rangle$ is the reduced dipole matrix element. The $d_{J'}$ are known to about 500 ppm precision from lifetime and photoassociation measurements [27].

Similarly, the tensor term is given by [13]

$$\alpha^{(2)}_{5P} = \frac{20}{\sqrt{21}} \sum_{J',F'} \frac{|d_{J'}|^2 \omega'}{\omega'^2 - \omega^2} (-1)^{F'} (2F'+1) \times \left\{ \begin{array}{ccc} 2 & 1 & F' \\ 1 & 2 & 2 \end{array} \right\} \left\{ \begin{array}{ccc} F' & 3/2 & J' \\ 1/2 & 1 & 2 \end{array} \right\}^2 . \quad (6)$$

Evaluating the ratio gives $\alpha^{(2)}/(d\alpha/d\lambda) = 538.5(4)$ fm, which is larger than the value determined from our fit by about 1.3σ. If we constrain the fit to use the calculated value for $\alpha^{(2)}/(d\alpha/d\lambda)$, we obtain $\lambda^{(0)} = 790.032352(29)$ nm, about 1σ different from the unconstrained result. The constrained fit gives a χ^2/d.o.f. of 1.2, compared to 0.5 for the unconstrained fit, both of which are reasonable. Since the calculated value for $\alpha^{(2)}/(d\alpha/d\lambda)$ is expected to be accurate, we report the value obtained from the constrained fit.

Our error estimate comes from a combination of statistical error and polarization drift, as discussed above. Another potential contribution is the calibration uncertainty in our wavelength measurement. We used a Bristol Instruments model 621A wave meter that displayed digits to 1 fm, with results repeatable to about 10 fm. We tested the meter by measuring four known saturated absorption lines in K, Rb, and Cs. The results indicated a calibration correction of -40(5) fm at a wavelength of 790 nm. This correction was applied to the data reported here. The wavelength calibration was performed both at the start and end of data collection, with no significant difference observed.

Another possible source of error is asymmetry in the Stark laser spectrum [5, 8]. The laser diode source produces broadband ASE light [20], which can be observed through its effect on the spontaneous emission rate of the atoms. The level thus deduced was large enough to potentially shift λ_0, but the effect could be controlled by spectral filtering with a 0.4 nm bandwidth. We implemented this with a diffraction grating and pinhole, and further verified that using a 0.2 nm bandwidth instead did not change our measurement results. Asymmetry in the tails of the laser line itself was ruled out at the 10^{-4} level within a bandwidth of 1 GHz, using an optical spectrum analyzer.

Other error effects considered include the Zeeman shifts from the trap field, non-uniformity of the trap field, dc background magnetic fields, atomic hyperpolarizability, atomic interactions, and alignment of the polarization angle to the trap field. None of these contributed any significant uncertainty to the result.

Our result disagrees considerably with the previous measurement by Lamporesi *et al.* of 790.018(2) nm [6], but those authors did not report a special effort to control the polarization so their result likely applies to some combination of the scalar and vector polarizabilities.

Our results can be compared to theory. We use the theoretical approach described in [4], with details explained in the Supplemental Material [21]. We obtain $\lambda^{(0)} = 790.0314(7)$ nm, where the error estimate primarily reflects uncertainty in the treatment of correlations. The measurement and calculation are in reasonable agreement.

We can also use our result to determine the matrix element ratio $R = |d_{3/2}/d_{1/2}|^2$ [5]. The scalar polarizability can be expressed

$$\alpha^{(0)} = A + |d_{1/2}|^2 \left(K_{1/2} + K_{3/2} R\right) \quad (7)$$

where A includes $\alpha_{\rm core}$ and contributions from all valence states above $5P$. Theory calculations yield $A = 10.70(12)$ au [21], and the experimental value for $d_{1/2}$ is 4.233(2) au [27]. The coefficients $K_{J'} \equiv \alpha^{(0)}_{5P_{J'}}/|d_{J'}|^2$ can be obtained from Eq. (5) and our result for $\lambda^{(0)}$. Setting $\alpha^{(0)} = 0$ and solving for R yields 1.99219(3). This is consistent with the ratio of the previous experimental matrix elements, $R = 1.995(3)$ [27], and with our theoretical estimate of 1.9917(5) [21]. The 15 ppm accuracy of our measurement is smaller than the calculated effects of the Breit interaction and QED corrections both of which increase R by about 50 ppm [21].

For both $\lambda^{(0)}$ and R, our experimental accuracy exceeds that of the theory by about an order of magnitude, and exceeds that of previous measurements by nearly two order of magnitudes. Our agreement with theory thus validates existing calculations to an extent not previously possible, and we hope that our improved precision will stimulate further progress. Testing the Breit and QED corrections would be particularly valuable as they are used when interpreting the parity violation experiments in Cs [14, 15].

In summary, the method we have described to measure the tune-out wavelength offers significantly improved precision and can provide very accurate values for matrix element ratios. The technique can be readily applied to other tune-out wavelengths in Rb, which we hope to pursue in future work. More generally the method could be used with any Bose-condensed atomic species.

Acknowledgments

We are grateful to A. Cronin for helpful discussions and comments on the manuscript, and to V. Dzuba for the use of his QED code. The Virginia group was supported by the National Science Foundation Grant No. 1312220, NASA Grant No. 1502012, and the Jefferson Scholars Foundation. This research was performed in part under the sponsorship of the US Department of Commerce, National Institute of Standards and Technology.

[1] H. Gould and T. M. Miller, in *Advances in Atomic, Molecular, and Optical Physics, Vol. 51*, edited by P. R. Berman, C. C. Lin, and H. Walther (Elsevier, Amsterdam, 2005), p. 343.

[2] J. Mitroy, M. S. Safronova, and C. W. Clark, J. Phys. B: At. Mol. Opt. Phys. **43**, 202001 (2010).

[3] L. J. LeBlanc and J. H. Thywissen, Phys. Rev. A **75**, 053612 (2007).

[4] B. Arora, M. S. Safronova, and C. W. Clark, Phys. Rev. A **84**, 043401 (2011).

[5] W. F. Holmgren, R. Trubko, I. Hromada, and A. D. Cronin, Phys. Rev. Lett. **109**, 243004 (2012).

[6] G. Lamporesi, J. Catani, G. Barontini, Y. Nishida, M. Inguscio, and F. Minardi, Phys. Rev. Lett. **104**, 153202 (2010).

[7] C. D. Herold, V. D. Vaidya, X. Li, S. L. Rolston, J. V. Porto, and M. S. Safronova, Phys. Rev. Lett. **109**, 243003 (2012).

[8] B. M. Henson, R. I. Khakimov, R. G. Dall, K. G. H. Baldwin, L.-Y. Tang, and A. G. Truscott, Phys. Rev. Lett. **TBP**, in press (2015).

[9] L. W. Clark, L.-C. Ha, C.-Y. Xu, and C. Chin (2015), arXiv:1506:01766 [cond-mat.quant.gas].

[10] P. Schneeweiss, F. L. Kien, and A. Rauschenbeutel, New J. Phys. **16**, 013014 (2014).

[11] R. Trubko, J. Greenberg, M. T. St Germaine, M. D. Gregoire, W. F. Holmgren, I. Hromada, and A. D. Cronin, Phys. Rev. Lett. **114**, 140404 (2015).

[27] D. A. Steck, available online at http://steck.us/alkalidata (revision 2.1.4).

[13] F. L. Kien, P. Schneeweiss, and A. Rauschenbeutel, Eur. Phys. J. D **67**, 92 (2013).

[14] V. V. Flambaum and J. S. M. Ginges, Phys. Rev. A **72**, 052115 (2005).

[15] V. A. Dzuba, V. V. Flambaum, and M. S. Safronova, Phys. Rev. A **73**, 022112 (2006).

[16] V. A. Dzuba and V. V. Flambaum, Int. J. Mod. Phys. E **21**, 1230010 (2012).

[17] M. S. Safronova, M. G. Kozlov, and C. W. Clark, IEEE Trans. Ultrason., Ferroelect., Freq. Control **59**, 439 (2012).

[18] J. H. T. Burke, B. Deissler, K. J. Hughes, and C. A. Sackett, Phys. Rev. A. **78**, 023619 (2008).

[19] K. J. Hughes, B. Deissler, J. H. T. Burke, and C. A. Sackett, Phys. Rev. A **76**, 035601 (2007).

[20] W. W. Chow and R. R. Craig, IEEE J. Quant. Elect. **16**, 1363 (1990).

[21] See Supplemental Material for a description of theoretical methods and results.

[22] M. S. Safronova and U. I. Safronova, Phys. Rev. A **83**, 052508 (2011).

[23] U. Volz and H. Schmoranzer, Physica Scripta T **65**, 48 (1996).

[24] M. S. Safronova and W. R. Johnson, Adv. At. Mol., Opt. Phys. **55**, 191 (2007).

[25] C. D. Herold, V. D. Vaidya, X. Li, S. L. Rolston, J. V. Porto, and M. S. Safronova, Phys. Rev. Lett. **109**, 243003 (2012).

[26] Kramida, A, Ralchenko, Yu, Reader, J, and NIST ASD Team (2012). NIST Atomic Spectra Database (ver. 5.0), [Online]. Available: http://physics.nist.gov/asd [2013, June 24]. National Institute of Standards and Technology, Gaithersburg, MD.

[27] D. A. Steck, available online at http://steck.us/alkalidata (revision 2.1.4).

[28] V. A. Dzuba, V. V. Flambaum, and M. S. Safronova, Phys. Rev. A **73**, 022112 (2006).

[29] V. V. Flambaum and J. Ginges, Phys. Rev. A **75**, 052115 (2005).

[30] S. G. Porsev, K. Beloy, and A. Derevianko, Phys. Rev. Lett. **102**, 181601 (2009).

Supplemental Material

We detail here the theoretical calculations referenced in the main paper. The ground state polarizability may be separated as

$$\alpha(\omega) = \alpha_c + \alpha_{vc} + \alpha_0(\omega),$$

where α_c is the contribution from the core electrons, α_{vc} is a modification of the core polarizability due to the valence electron, and α_0 is the contribution from the valence electron. The two core terms are approximately static and are calculated in the random-phase approximation [22]. The valence term for the 5s state is determined using the sum-over-states formula

$$\alpha_0(\omega) = \frac{1}{3}\sum_k \frac{\langle k \,\|d\|\, 5s\rangle^2 (E_k - E_{5s})}{(E_k - E_{5s})^2 - \omega^2}, \qquad (8)$$

where $k = np_{1/2}$ and $np_{3/2}$. Up to $n = 12$ we evaluate discrete terms in this sum using experimental values for the state energies E. Experimental matrix elements from Ref. [23] are used for the $5s - 6p$ transitions while all other matrix elements use the all-order calculations of [22]. The details of the methods are discussed in [24]. While experimental values are available for the 5s-5p matrix elements [23], the theoretical values are estimated to have a more accurate ratio, which is most important here. For $n > 12$, the remaining 'tail' contributions are calculated in the Dirac-Hartree-Fock approximation. The state energies and matrix elements are listed in Table I. Using these values, the tune-out wavelength is predicted to lie at $\lambda^{(0)} = 790.02568$ nm as indicated. This value does not include the effects of hyperfine structure.

The uncertainty in the theoretical value is dominated by uncertainty in the 5p matrix elements. For instance, the estimated uncertainty in α from all of the non-5p contributions is about 0.2 au. Via the derivative $d\lambda/d\alpha = -397$ fm/au, this leads to a wavelength error of 80 fm. The net value of the non-5p contributions does give a significant shift of -4.2 pm, mainly from the core polarizability.

As noted, the 5p matrix elements themselves contribute primarily through their ratio

$$R = \frac{\langle 5s||d||5p_{3/2}\rangle^2}{\langle 5s||d||5p_{1/2}\rangle^2}. \qquad (9)$$

This is useful, because the theoretical accuracy of the ratio is better than that of the individual matrix elements since a large fraction of the correlation corrections cancel. This can be seen in Table II, where we compare the matrix elements obtained using various approximations [22]. All of the methods are intrinsically relativistic. The calculations in Table II of the tune-out wavelength differ only in the values of these two matrix elements, with all other values taken from Table I.

TABLE I: Breakdown of the contributions to the $5s$ polarizability in Rb at $\lambda = 790.02568$ nm. Reduced matrix elements d and polarizability contributions are given in atomic units. Experimental matrix elements from Ref. [25] are used for the $5s-6p$ transitions; remaining matrix elements are from the all-order calculations [22, 25]. Uncertainties are given in parenthesis. Experimental energies ΔE are measured from the ground state and given in cm^{-1} [26].

Contr.	ΔE	d	α_0
$5p_{1/2}$	12578.951	4.2199	-8233.6
$6p_{1/2}$	23715.081	0.3235(9)	0.451(3)
$7p_{1/2}$	27835.05	0.115(3)	0.044(2)
$8p_{1/2}$	29834.96	0.060(2)	0.011(1)
$9p_{1/2}$	30958.91	0.037(3)	0.004(1)
$10p_{1/2}$	31653.85	0.026(2)	0.002
$11p_{1/2}$	32113.55	0.020(1)	0.001
$12p_{1/2}$	32433.50	0.016(1)	0.001
$(>12)p_{1/2}$			0.022(22)
$5p_{3/2}$	12816.54939	5.9550	8222.9
$6p_{3/2}$	23792.591	0.5230(8)	1.173(4)
$7p_{3/2}$	27870.14	0.202(4)	0.135(6)
$8p_{3/2}$	29853.82	0.111(3)	0.037(2)
$9p_{3/2}$	30970.19	0.073(5)	0.015(2)
$10p_{3/2}$	31661.16	0.053(4)	0.008(1)
$11p_{3/2}$	32118.52	0.040(3)	0.004(1)
$12p_{3/2}$	32437.04	0.033(2)	0.003
$(n>12)_{3/2}$			0.075(75)
Core + vc			8.709(93)
Total			0.001

The most accurate methods are expected to be the four all-order calculations SD, SDpT, SD_{sc}, and SDpT_{sc}. We take the average of these as the final theoretical values, and use them to calculate

$$R = 1.9917(5)$$

and

$$\lambda^{(0)} = 790.0261(7)\mathrm{nm}.$$

The uncertainty is estimated from the spread in the four values. While the scaling (SD_{sc}, and SDpT_{sc}) technique is supposed to account for a class of missing correlation effects, the scaling affects only about half of the correlation correction in this transition. Therefore we use the full spread of the values as our error estimate to allow for the effects missed by scaling. We note that this uncertainty estimation is approximate since we are attempting to account for unknown correlation effects due to triple, quadrupole, and higher excitations.

None of the matrix element values in Table II include Breit or QED corrections. We evaluate the importance of these effects in the lowest-order DF approximation and summarize the resulting values in Table III. First, we

TABLE II: Reduced electric-dipole matrix elements for the $5s-5p_j$ transitions [22], their ratio R (see Eq. (9)), and corresponding values of the tune-out wavelength $\lambda^{(0)}$ (nm). Theoretical methods: DF is the lowest-order Dirac-Hartree-Fock, II and III are second- and third-order many-body perturbation theory values, SD and SDpT are *ab initio* all-order values calculated in the single-double approximation and with inclusion of the partial triple contributions, and SD_{sc}, SDpT_{sc} are corresponding scaled all-order values. Experimental values are averages of several measurements compiled in [27]. The experimental errors differ from those in Steck; we calculated them as $\sigma_{avg} = (\sum_i \sigma_i^{-2})^{-1/2}$. The error in the experimental $\lambda^{(0)}$ is obtained by varying R by 1σ.

	DF	II	III	SD	SD_{sc}	SDpT	SDpT_{sc}	Expt.
$5s-5p_{1/2}$	4.8189	4.5981	4.1855	4.2199	4.2535	4.2652	4.2498	4.233(2)
$5s-5p_{3/2}$	6.8017	6.4952	5.9047	5.955	6.0031	6.0196	5.9976	5.978(4)
R	1.9922	1.9954	1.9902	1.9914	1.9919	1.9918	1.9917	1.995(3)
$\lambda^{(0)}$	790.02603	790.03155	790.02380	790.02568	790.02636	790.02632	790.02607	790.031(6)

TABLE III: Reduced electric-dipole matrix elements for the $5s-5p_j$ transitions and the corresponding line strength ratio R.

	DF	DF+Breit	DF+QED
$5s-5p_{1/2}$	4.8189	4.8192	4.82038
$5s-5p_{3/2}$	6.8017	6.8023	6.80384
R	1.9922	1.9923	1.9923

carry out the DF calculation with the Breit interaction included on the same footing with the Coulomb interaction (see, for example, Ref. [28]). The resulting values are listed in the column labeled "DF+Breit." Then, we carry out the DF calculation with the inclusion of the QED model potential, constructed as described in Ref. [29]. The Breit interaction is excluded in this calculation to separate the two effects. We find that both Breit and QED corrections are five times smaller than our uncertainty in the correlation contribution to the ratio.

While the experimentally extracted ratio $R = 1.99219(3)$ can be directly compared to the theoretical value $R = 1.9917(5)$, it is also instructive to compare the tune-out wavelengths. At the level of the theoretical accuracy, it is only necessary to account for the ground state hyperfine shift, so we simply recalculate the tune-out wavelength with modified energy levels $\Delta E(5s-5p_{1/2}) = 12578.8655$ cm^{-1} and $\Delta E(5s-5p_{3/2}) = 12816.4639$ cm^{-1}. This yields 790.0314(7) nm, in reasonable agreement with the experimental value of 790.032352(29) nm. We use the same theoretical uncertainty as for the value with no hyperfine interaction.

We highlight three important conclusions regarding the theoretical impact of our results:

First, the procedure to estimate the theoretical uncertainty is confirmed to be reasonably accurate, since theory agrees with the more precise experiment to about the theoretical 1σ estimate.

Second, we see that the ratio of matrix elements can be a useful measure of the accuracy of theoretical approaches beyond DF. Note that the second-order and third-order values in Table II are outside of the theory uncertainty estimate, and disagree significantly with the experimental result. These methods are expected to be less accurate than all-order techniques.

Third, the accuracy of the experimental value is sufficient to test the Breit and QED effects if a more accurate correlation treatment of the ratio is carried out. It may be possible to achieve this in the full triple coupled-cluster approach used to treat Cs parity violation [30]. If successful, this would help support the results obtained for Cs.